Experimental and Theoretical ^{17}O NMR Study of the Influence of Hydrogen-Bonding on C═O and O−H Oxygens in Carboxylic Solids

Alan Wong,[†] Kevin J. Pike,[†,||] Rob Jenkins,[‡] Guy J. Clarkson,[‡] Tiit Anupõld,[§] Andrew P. Howes,[†] David H. G. Crout,[‡] Ago Samoson,[§] Ray Dupree,[†] and Mark E. Smith*[,†]

Department of Physics, University of Warwick, Coventry, CV4 7AL, U. K., Department of Chemistry, University of Warwick, Coventry, CV4 7AL, U. K., and National Institute for Chemical Physics and Biophysics, Akadeemia Tee 23, Tallinn, Estonia

Received: October 11, 2005; In Final Form: December 1, 2005

A systematic solid-state ^{17}O NMR study of a series of carboxylic compounds, maleic acid, chloromaleic acid, KH maleate, KH chloromaleate, K_2 chloromaleate, and LiH phthalate·MeOH, is reported. Magic-angle spinning (MAS), triple-quantum (3Q) MAS, and double angle rotation (DOR) ^{17}O NMR spectra were recorded at high magnetic fields (14.1 and 18.8 T). ^{17}O MAS NMR for metal-free carboxylic acids and metal-containing carboxylic salts show featured spectra and demonstrate that this combined, where necessary, with DOR and 3QMAS, can yield site-specific information for samples containing multiple oxygen sites. In addition to ^{17}O NMR spectroscopy, extensive quantum mechanical calculations were carried out to explore the influence of hydrogen bonding at these oxygen sites. B3LYP/6-311G++(d,p) calculations of ^{17}O NMR parameters yielded good agreement with the experimental values. Linear correlations are observed between the calculated ^{17}O NMR parameters and the hydrogen bond strengths, suggesting the possibility of estimating H-bonding information from ^{17}O NMR data. The calculations also revealed intermolecular H-bond effects on the ^{17}O NMR shielding tensors. It is found that the δ_{11} and δ_{22} components of the chemical shift tensor at O−H and C═O, respectively, are aligned nearly parallel with the strong H-bond and shift away from this direction as the H-bond interaction weakens.

1. Introduction

NMR spectroscopy of ^{1}H, ^{13}C, and ^{15}N nuclei has become an important tool for studying biomolecular structures.[1] Despite the fact that oxygen is also an abundant element in biological molecules, only a handful of ^{17}O NMR studies are found in the literature.[2,3] The lack of experimental ^{17}O NMR data is related to the fact that for the ^{17}O nucleus it is intrinsically difficult to obtain high-resolution NMR spectra. Two major factors contribute to the difficulty: (i) the low natural abundance of ^{17}O (0.037%) and (ii) the quadrupole interaction associated with oxygen. Very often this quadrupole interaction gives rise to broad NMR signals that limit the ability to yield site-specific information, especially for large molecules. As a result, mainly solution ^{17}O studies have been reported for small organic molecules.[3] However, the limitation of solution ^{17}O NMR studies of larger molecules arises from the fast relaxation of ^{17}O nuclei and/or exchange. This is one of the reasons that few solution ^{17}O NMR studies have been reported on large biological systems. Fortunately, such fast relaxation is not a limiting factor in solid-state ^{17}O NMR spectroscopy.[2,4]

^{17}O NMR studies of solids are still relatively scarce. However, for inorganic solids, there have been great strides since the original work by the Oldfield group[5] and natural abundance studies of simple oxides by Bastow and Stuart.[6] In ionic materials, the electrical field gradients (EFGs) at the oxygen sites tend to be small, resulting in intrinsically high-resolution magic-angle spinning (MAS) ^{17}O NMR spectra.[6−8] For the important case of silicates and aluminosilicates, the quadrupolar interaction increases as the bond covalent character increases.[8] As a result, the MAS spectrum is broadened and high-resolution techniques such as double angle rotation (DOR) and multiple quantum (MQ) are often required. ^{17}O NMR has been reported in crystalline silicates[9] and glasses,[10] sol−gel prepared materials,[11] and siliceous zeolites[12] with more recent ^{17}O studies of borates, borosilicates and boroaluminosilicates,[13] and phosphates[14] where there is a further increase in the quadrupolar interaction.

The extension of ^{17}O NMR to organic solids is an even greater challenge, as the quadrupole interaction tends to be larger than that for inorganic materials. Several groups have reported solid-state ^{17}O NMR studies of organic/bio-organic systems. In particular, Fiat and co-workers recorded solid-state ^{17}O NMR signals for amino acids.[15] Oldfield and co-workers applied solid-state ^{17}O NMR to probe heme proteins and model compounds.[16] Very recently, high-field ^{17}O spectra of membrane proteins WALP-23[17] (at 18.8 T) and gramicidin A[18] (at 21 T) have also been reported. Ando and co-workers used solid-state ^{17}O NMR to study H-bonding interactions in polypeptides.[19] Single-crystal ^{17}O NMR studies of a few organic solids have also been reported.[20,21] Recently, Wu and co-workers[22−27] used a combination of solid-state ^{17}O NMR and quantum mechanical calculations to investigate the oxygen sites in organic materials. The ^{17}O NMR information was somewhat limited because of the poor spectral resolution. Conventional MAS spectra can be difficult to analyze especially when a system contains multiple sites that strongly overlap in the spectrum. This overlap is due to the second-order quadrupole interaction not being completely

* To whom correspondence should be addressed. E-mail: M.E.Smith.1@warwick.ac.uk.
[†] Department of Physics, University of Warwick.
[‡] Department of Chemistry, University of Warwick.
[§] National Institute for Chemical Physics and Biophysics.
[||] Present address: NMR Group, ANSTO, New Illawarra Road, Lucas Heights, NSW 2234, Australia.

10.1021/jp055807y CCC: $33.50
Published on Web 01/10/2006

CHART 1. Molecular Structure of the Carboxylic Compounds Studied Here

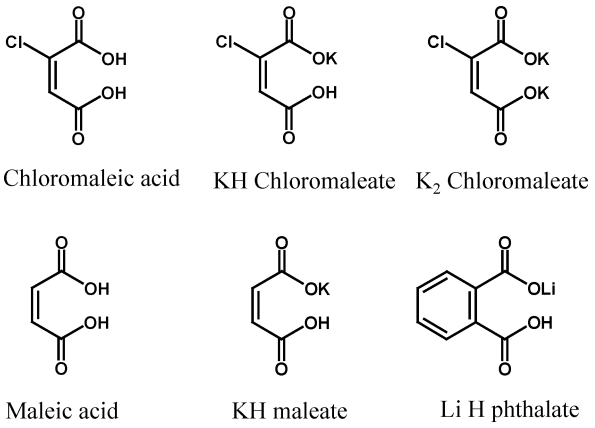

averaged by traditional MAS. Various more modern NMR techniques such as dynamic-angle spinning (DAS),[28] DOR,[29] and MQMAS[30] were developed for achieving high resolution for half-integer quadrupolar nuclei such as ^{17}O. The first two-dimensional (2D) ^{17}O MQMAS and DAS for organic materials were reported by Wu et al.[31] and Gann et al.,[32] respectively. Recently, ^{17}O DOR has been reported on amino acids[33] and glutamic acid[34] and ^{17}O MAS on phthalate compounds.[35]

Theoretical calculations of ^{17}O NMR parameters have proven to be a good complementary tool to solid-state ^{17}O NMR spectroscopy, not only to assist in spectral assignments for complicated ^{17}O NMR spectra but also to help understand the structural influences on the NMR parameters. Wu and co-workers[22−27] carried out extensive quantum chemical calculations of ^{17}O EFG and chemical shielding tensors on "molecular clusters" of organic compounds. They showed that both restricted Hartree−Fock (RHF) and density functional theory (DFT) levels gave good agreement with the experimental values. Bryce et al.[36] also reported good agreement between the DFT calculations and experimental values of ^{17}O NMR parameters of phosphine-oxide compounds. Recently, Yates et al.[37] used a different method to calculate the ^{17}O NMR parameters of the oxygen sites of glutamic acid polymorphs. Rather than estimating the ^{17}O NMR parameters of the target oxygen in a molecular cluster,[22−27,36] the calculations were carried out for the full crystal structure. The calculated results were in good agreement with experiment. An advantage of using traditional cluster DFT calculations is the structural flexibility for studying model systems.

It is known that carboxylic acids play important functional roles in biological molecules. Many molecules significant in biological processes contain carboxylic groups, including amino acids and fatty acids. For these reasons, it is important to be able to probe the oxygen sites of the carboxylic groups and study their hydrogen bonding. As an initial model for an ^{17}O NMR study of carboxylic compounds, a series of crystallographically well-defined molecules with strong O···H−O hydrogen bonding have been chosen:[38] maleic acid, chloromaleic acid, KH maleate, KH chloromaleate, K_2 chloromaleate, and LiH phthalate; see Chart 1. High-resolution ^{17}O (MAS, MQMAS, and DOR) NMR spectroscopy and quantum mechanical calculations are combined to study the influence of H-bonds on ^{17}O NMR parameters in these compounds.

2. Experimental Section

Sample Preparation. In general, ^{17}O enrichment was achieved by dissolving nonenriched anhydrides of the carboxylic acids in $H_2{}^{17}O$ (10% ^{17}O, Cambridge Isotopes Laboratories), dioxane (ca. 1:1). The solution was then acidified with HCl(g) at gentle heat for a couple of hours. The sample was then lyophilized to recover the $H_2{}^{17}O$/dioxane solvent, and the residual acids were used directly for this study.

X-ray Crystallography. Crystallographic and diffraction data for chloromaleic acid were collected at 180 K on a Siemens P4 single-crystal diffractometer with graphite-monochromated Mo Kα radiation. Data were corrected for Lorentz and polarization effects and analyzed using Siemens SHELXTL software package.[39]

Solid-State ^{17}O NMR. Most solid-state ^{17}O NMR spectra were recorded on a Chemagnetics Infinity 600 spectrometer at an applied magnetic field of 14.1 T operating at a frequency of 81.345 MHz. Some additional ^{17}O MAS spectra were acquired at magnetic fields of 8.45 and 18.8 T, with the spectrometers operating at 48.8 and 108.4 MHz, respectively. A 4 mm MAS probe was used for ^{17}O MAS and 3QMAS experiments. The sample spinning frequency was controlled to be 14000−18000 ± 10 Hz. A spin−echo experiment[40] was used to record all ^{17}O MAS spectra with the echo delay set to an integer number of rotor periods. Approximately 20 000 transients were recorded with a recycle delay of 2−10 s. The radio frequency field strength at the ^{17}O frequency was ca. 67 kHz. "Solid" 90° and 180° pulses were used. All spectra were referenced to water at 0.0 ppm. The ^{17}O MAS spectra were processed using WinNuts,[41] and the spectral simulations were performed with WSOLIDS.[42]

Split-t_1 MQMAS[43] was used for recording the ^{17}O 3QMAS spectra. The sample spinning frequency was set to 15 kHz. The optimized excitation and conversion pulse widths were 5.2 and 1.2 μs, respectively, with a t_1 offset of 2.0 μs. Further experimental details are reported in the figure captions. ^{17}O DOR NMR experiments were carried out using odd-order sideband suppression,[44] and the outer rotor speed was varied between 1300 and 1700 Hz to determine the centerband.

Computational Aspects. All quantum mechanical calculations were performed on a SunFire 6800 symmetric multiprocessor system (24 × 900 MHz processors and 24 GB of memory) using the Gaussian98 suite of programs.[45] The experimental X-ray structures are directly used without any geometry optimization, and molecular clusters were used in the calculations. In general, the cluster is built upon the target oxygen site. The cluster consists of all the first-coordination ligands, solvent molecules, or metal ions that directly interact with the target oxygen. For oxalic acid, second-coordination species were also included in the cluster. The typical number of atoms in a cluster ranges from 25 to 95, depending on the local environment of the target oxygen site. For the carboxylic compounds examined in this study, the calculations were performed at the DFT level with a 6-311++G(d,p) basis set. The principal components of the ^{17}O EFG tensor, q_{ii}, were computed in atomic units (1 au = 9.717365×10^{21} V m^{-2}), with $|q_{zz}| > |q_{yy}| > |q_{xx}|$ and $q_{zz} + q_{yy} + q_{xx} = 0$. The principal magnetic shielding tensor components (σ_{ii}) were computed with $\sigma_{iso} = (\sigma_{11} + \sigma_{22} + \sigma_{33})/3$ and $\sigma_{33} > \sigma_{22} > \sigma_{11}$.

To make a direct comparison between the calculated ^{17}O NMR parameters (quadrupolar coupling constanst (χ_q), asymmetry parameter (η_q), and isotropic chemical shift (δ_{iso})) and the experimental results from the NMR powder samples,[46] the following equations were used

$$\chi_q\,(\mathrm{MHz}) = e^2 q_{zz} Q/h = -243.96 Q(\mathrm{barn}) q_{zz}(\mathrm{au}) \quad (1)$$

$$\eta_q = (q_{xx} - q_{yy})/q_{zz} \quad (2)$$

$$\delta_{iso} = \sigma_{ref} - \sigma_{iso} \quad (3)$$

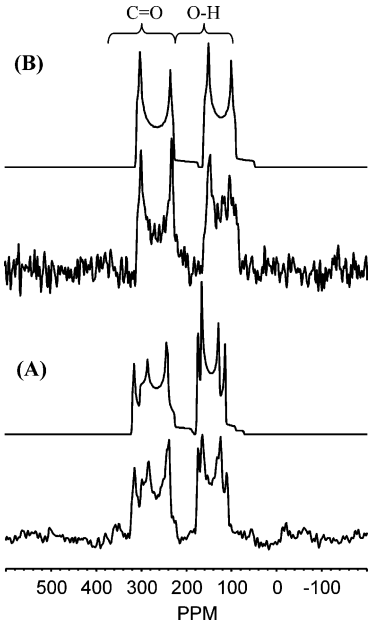

Figure 1. Experimental (bottom) and simulated (upper) ^{17}O MAS spectra at 14.1 T for (A) maleic acid and (B) chloromaleic acid.

where Q is the nuclear quadrupole moment, e is the elementary electronic charge, h is the Planck constant, and σ_{ref} is the magnetic shielding constant for the primary chemical shift reference sample. A Q value of -0.0255 barns[47] together with an absolute shielding reference $\sigma_{ref} = 287.5$ ppm[48] were used.

3. Results and Discussion

Solid-State ^{17}O NMR of Carboxylic Acids. In general, a metal-free carboxylic acid consists of two different types of oxygen atom, carbonyl (C═O) and hydroxyl (O−H). With the different C−O bonding characteristics, one would expect that the two types of oxygen would have distinct ^{17}O resonances in NMR spectroscopy. As shown in Figure 1, the ^{17}O MAS spectra for maleic and chloromaleic acids exhibit two well-separated sets of resonances, both show typical second-order quadrupolar broadened central transition line shapes. In general, it is found that δ_{iso} for the C═O oxygen sites in carboxylic acids appears at 310−340 ppm, whereas a more upfield position between 170 and 190 ppm is observed for the O−H sites. The χ_q values for C═O oxygen are found to be 7.0−8.5 MHz and 6.5−7.5 MHz for O−H oxygen. These spectral assignments for C═O and O−H sites are in agreement with previously reported values from amino acids,[33,49] phthalic acid,[35] and glutamic acid.[34] From spectral simulations, ^{17}O NMR parameters (δ_{iso}, χ_q, and η_q) were deduced with good accuracy and tabulated in Table 1.

As shown in Figure 2A, there are four crystallographically distinct oxygen sites in maleic acid:[50] two C═O and two O−H. The difference in these oxygen sites arises from the coexistence of two different H-bonding interactions in maleic acid: intra- and intermolecular interactions. The intramolecular H-bonding (C═O1···H−O4) exhibits a stronger bond, with a distance of 1.596 Å, than that of the intermolecular H-bonding (C═O3···H−O2′), 1.661 Å apart. Consequently, the ^{17}O MAS spectrum shown in Figure 1A exhibits two sets of second-order quadrupole line shapes, each with well-defined singularities, for both C═O and O−H. On the basis of those well-defined signal singularities, the ^{17}O NMR parameters of the four different oxygen sites were determined from a spectral simulation: [C═O1] $\delta_{iso} = 312 \pm 2$ ppm, $\chi_q = 7.40 \pm 0.05$ MHz, and $\eta_q = 0.24 \pm 0.05$; [C═O3] $\delta_{iso} = 339 \pm 2$ ppm, $\chi_q = 8.30 \pm 0.05$ MHz, and $\eta_q = 0.05 \pm 0.05$; [O4−H] $\delta_{iso} = 182 \pm 2$ ppm, $\chi_q = 6.98 \pm 0.05$ MHz, and $\eta_q = 0.00 \pm 0.05$; [O2−H] $\delta_{iso} = 189 \pm 2$ ppm, $\chi_q = 6.60 \pm 0.05$ MHz, and $\eta_q = 0.05 \pm 0.05$. The above assignments are based on the quantum mechanical calculation of ^{17}O chemical shielding and EFG which will be discussed later.

Figure 1B shows the ^{17}O MAS NMR spectrum of chloromaleic acid which exhibits similar spectral features to that of maleic acid (Figure 1A) (but with no splitting of the lines) and the ^{17}O MAS spectrum previously reported for phthalic acid.[35] The ^{17}O NMR parameters were found to be the following: [C═O] $\delta_{iso} = 329 \pm 5$ ppm, $\chi_q = 8.28 \pm 0.10$ MHz, and $\eta_q = 0.10 \pm 0.05$; [O−H] $\delta_{iso} = 175 \pm 5$ ppm, $\chi_q = 7.45 \pm 0.10$ MHz, and $\eta_q = 0.15 \pm 0.05$. Unfortunately, there is no crystal structure reported for chloromaleic acid. As a result, the structure was determined. Details of the crystallographic and structural data are reported in CIF format as Supporting Information. It was found to crystallize in a primitive monoclinic cell, space group $P2_1/C$, with lattice parameters of $a = 7.558(2)$ Å, $b = 4.982(1)$ Å, $c = 16.015(4)$ Å, $\beta = 92.395(6)°$ with $Z = 4$. As seen in Figure 2B, the crystal structure of chloromaleic acid is similar to that found for phthalic acid;[35] it consists of two sets of similar intermolecular H-bonds with a C═O5···H−O6″ distance of 1.737 Å and C═O2···H−O1′ distance of 1.768 Å. The ^{17}O MAS NMR spectrum (Figure 1B) could not resolve the two sets of intermolecular H-bonds, which might be expected as the ^{17}O parameters of C═O and O−H oxygens should be similar for the two intermolecular H-bonds.

Solid-State ^{17}O NMR of Carboxylic Salts. Figure 3 displays a series of ^{17}O MAS spectra at 14.1 T for carboxylic compounds containing metal ions: KH maleate, KH chloromaleate, LiH phthalate·MeOH, and K_2 chloromaleate. The ^{17}O NMR parameters deduced from the simulations are reported in Table 1.

The carboxylate salts show changes in the ^{17}O MAS NMR spectra (Figure 3), suggesting that the local environments of the oxygen sites are different from those in carboxylic acids. This is probably a result of the oxygens having additional electrostatic interactions with the neighboring metal ions in the crystal lattice. For example, as shown in Figure 4, the crystal structures for KH maleate[52] and KH chloromaleate[53] reveal similar H-bonding motifs. Both consist of intramolecular H-bondings between an O−H oxygen and an anion oxygen (O^-), with O···O distances of 2.436 and 2.402 Å, respectively. In addition to H-bonds, C═O and O−H oxygens also interact with the neighboring potassium ions. In KH maleate, the average C═O···K and H−O···K distances are 2.95 and 2.86 Å, respectively, whereas in KH chloromaleate the corresponding distances are 2.83 and 3.03 Å. Consequently, as shown in Figure 3, the resonances for the C═O and O−H oxygens overlap with one another. The assignments of the resonances are based on various results: (1) relative signal intensity, (2) ^{17}O NMR calculations, and (3) ^{17}O DOR data. For KH maleate, the corresponding parameters were found to be the following [C═O] $\delta_{iso} = 322 \pm 2$ ppm, $\chi_q = 8.30 \pm 0.05$ MHz, and $\eta_q = 0.16 \pm 0.05$; [O−H] $\delta_{iso} = 235 \pm 2$ ppm, $\chi_q = 5.90 \pm 0.05$ MHz, and $\eta_q = 0.60 \pm 0.05$. For KH chloromaleate: [C═O1] $\delta_{iso} = 315 \pm 2$ ppm, $\chi_q = 8.35 \pm 0.05$ MHz, and $\eta_q = 0.16 \pm 0.05$; [C═O4] $\delta_{iso} = 317 \pm 2$ ppm, $\chi_q = 8.35 \pm 0.05$ MHz, and $\eta_q = 0.16 \pm 0.05$; [O−H] $\delta_{iso} = 228 \pm 2$ ppm, $\chi_q = 6.00 \pm 0.05$ MHz, and $\eta_q = 0.70 \pm 0.05$.

Although the ^{17}O NMR parameters for the potassium carboxylic salts can be determined from spectral simulations of the observed overlapping MAS resonances at 14.1 T, it would be better to resolve the resonances, C═O and O−H, in an NMR

TABLE 1: Experimental ^{17}O NMR Parameters for Carboxylic Compounds[a]

carboxylic compounds	site	δ_{iso}/±2 ppm	χ_q/±0.05 MHz	η_q/±0.05	relative intensity[b]	ref[c]
maleic acid	C═O1	312	7.40	0.24	0.25	*d*
	O4−H	182	6.98	0.00	0.25	*d*
	C═O3	339	8.30	0.05	0.25	*d*
	O2−H	189	6.60	0.05	0.25	*d*
chloromaleic acid[e]	C═O	329	8.28	0.10	0.50	*d*
	O−H	175	7.45	0.15	0.50	*d*
KH maleate	C═O	322	8.30	0.16	0.50	*d*
	O−H	235	5.90	0.60	0.50	*d*
KH chloromaleate	C═O1	315	8.35	0.16	0.25	*d*
	C═O4	317	8.35	0.16	0.25	*d*
	O−H	228	6.00	0.70	0.50	*d*
K_2 chloromaleate	O═C1═O	288	7.20	0.40	0.50	*d*
	O═C2═O	283	7.20	0.45	0.50	*d*
LiH phthalate·MeOH[e]	C═O	273	7.4	0.30	0.50	*d*
	O−H	225	6.5	0.25	0.50	*d*
phthalic acid[e]	C═O	312	7.2	0.05		35
	O−H	180	7.4	0.05		35
oxalic acid·$2H_2O$	C═O	301 ± 14	8.30 ± 0.23	0.07 ± 0.13		21
	O−H	183 ± 4	6.68 ± 0.08	0.16 ± 0.10		21
KH dibenzoate	C═O	287	8.30	0.23		27
	O−H	213	5.90	0.55		27

[a] Results are obtained from ^{17}O MAS. [b] Since the spinning sidebands in ^{17}O MAS spectra are small and negligible, the centerbands are normalized to a total intensity of 1. [c] Reference where parameters reported. [d] This work. [e] These spectra have a lower signal-to-noise or a less well-defined line shape. The experimental errors are larger: δ_{iso}, ±5 ppm; χ_q, ±0.1 MHz; η_q, ±0.1.

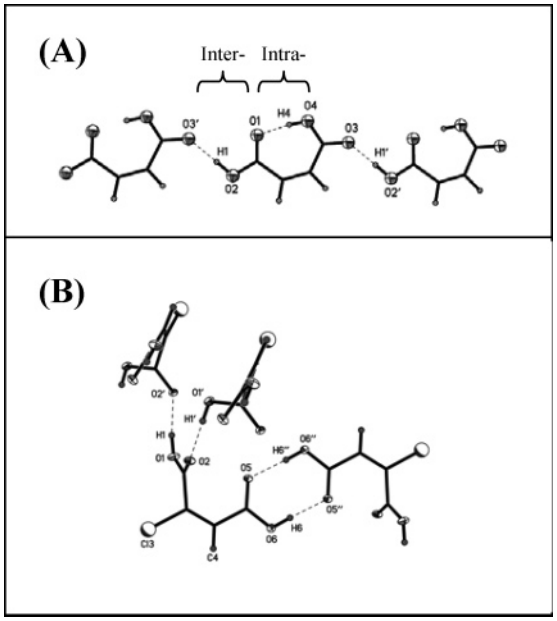

Figure 2. Crystal structure of (A) maleic acid, displaying both inter- and intramolecular hydrogen bonding and (B) chloromaleic acid. Crystallographic and structural data of chloromaleic acid are reported in CIF format as Supporting Information.

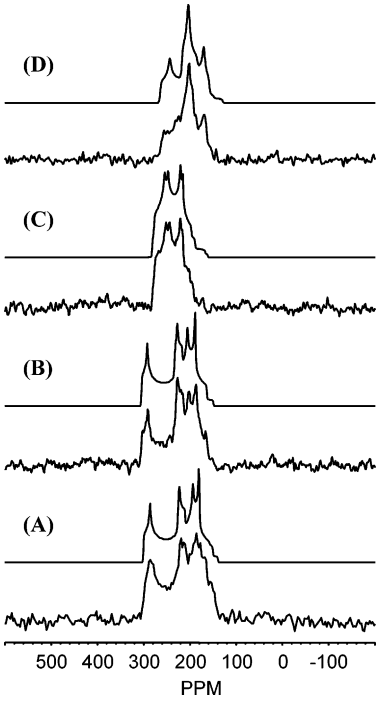

Figure 3. Experimental (bottom) and simulated (upper) ^{17}O MAS spectra at 14.1 T for (A) KH chloromaleate, (B) KH maleate, (C) K_2 chloromaleate, and (D) LiH phthalate·MeOH.

spectrum. To improve the MAS spectral resolution, a ^{17}O MAS spectrum for KH maleate was recorded at 18.8 T and, for comparison, at 8.45 T. As seen in Figure 5, it is difficult to extract accurate ^{17}O NMR data from the MAS spectrum recorded at 8.45 T because of the strong overlap of the C═O and O−H resonances. In contrast, these resonances are well separated at 18.8 T, allowing one to readily deduce accurate ^{17}O NMR information illustrating the advantage of using a higher field.[46]

For KH chloromaleate, the 3QMAS spectrum was recorded and shown in Figure 6. The projection of the F_2 axis produces a conventional 1D MAS spectrum, whereas the projection of F_1 corresponds to the isotropic axis. As seen in Figure 6A, there are two sharp signals at 204 and 223 ± 2 ppm in the isotropic dimension, corresponding to the C═O and O−H oxygens, respectively. Each isotropic 3Q resonance is also flanked by a set of spinning sidebands (ssb's). The line widths of the 3Q resonances for C═O and O−H are found to be ~700 and 1200 Hz, respectively. These values are much narrower than the MAS spectra shown in Figure 3A (12 000 and 6500 Hz for C═O and O−H, respectively). In 3QMAS experiments, the efficiency for both 3Q generation and 3Q-to-1Q conversion during the experiment is dependent on the strength of the quadrupolar interaction (χ_q) and the applied field.[8,30] As reported in Table 1, the χ_q values for C═O and O−H in KH chloromaleate are found to be 8.35 and 6.00 MHz, respectively, a difference of ~30%. This difference in χ_q results in a significant imbalance in 3Q generation and 3Q-to-1Q conversion. The 3QMAS

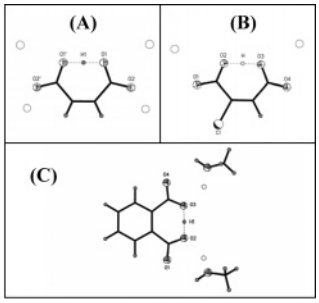

Figure 4. Crystal structures displaying the H-bonding in (A) KH maleate, (B) KH chloromaleate, and (C) LiH phthalate·MeOH. Metal ions are represented by the open circles.

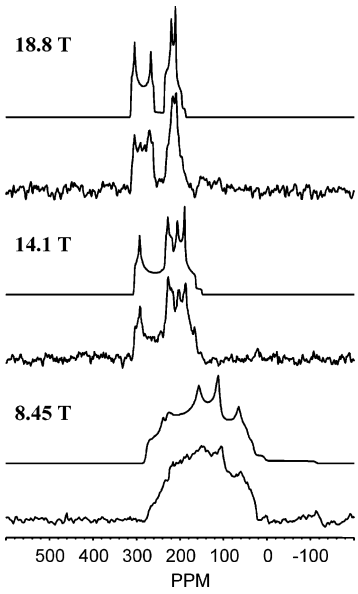

Figure 5. Experimental (bottom) and simulated (upper) ^{17}O MAS spectra of KH maleate at various applied magnetic fields.

spectrum in Figure 6B shows that the signal-to-noise (S/N) ratios for the C═O and O−H sites are quite different, where the resonance for C═O is weaker compared to that for O−H. As shown in Figure 6C, the S/N ratios of both C═O and O−H resonances are significantly improved by adding together the centerband and the first ssb's on either side. The MAS projections exhibit typical second-order quadrupolar line shapes, with an axial asymmetry parameter observed for the C═O oxygen and nonaxial asymmetry for O−H, in agreement with the full ^{17}O MAS spectrum.

In KH chloromaleate, the crystal structure has two C═O (O1 and O4) oxygens in slightly different environments.[53] The carbonyl C═O1 and C═O4 bond distances are 1.226 and 1.243 Å, respectively. This is attributed to the position of the neighboring chlorine, where the chlorine is attached to C2 and is only three bonds from the O1 oxygen. One would expect that the difference in C═O bond length would give rise to different ^{17}O NMR resonances. However, only one C═O resonance is observed in ^{17}O MAS and 3QMAS spectra. To attempt to resolve the two different C═O oxygen sites in KH chloromaleate, ^{17}O DOR spectra were recorded at 14.1 T. For comparison, a DOR spectrum for KH maleate was also obtained. The ^{17}O DOR spectra are shown in parts A and B of Figure 7, and the results are summarized in Table 2. For KH maleate, the DOR spectrum (Figure 7B) exhibits a single sharp isotropic signal at 256.3 ± 0.5 ppm flanked by a series of ssb's assigned to the C═O oxygens. The line width is found to be 80 Hz, ∼200 times narrower than that of the MAS signal. The broad signal

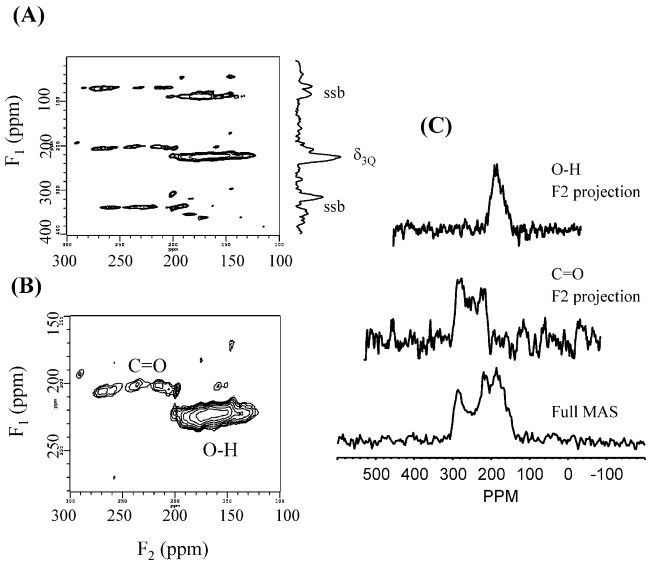

Figure 6. ^{17}O 3QMAS spectra for KH chloromaleate at 14.1 T: (A) Large spectrum showing two sets of spinning sidebands (ssb's) and the 3Q isotropic signal. (B) Expansion that displays only the 3Q isotropic resonances. (C) The F_2 projection of the spectral summation of the two ssb's and the centerband. Experimental details: the number of t_1 increments was 48 with a dwell time of 30 μs. The spectral widths were 50 and 200 kHz for F_2 and F_1, respectively. A total of 2400 transients were accumulated for each t_1 increment with a recycle delay of 5 s.

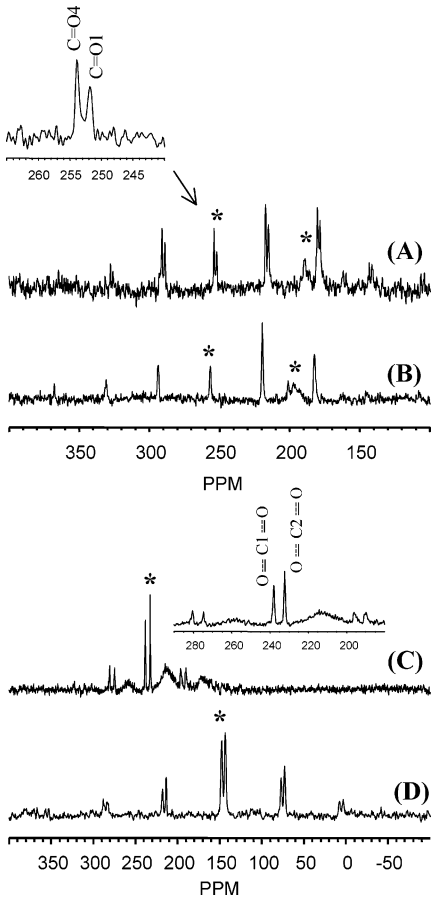

Figure 7. ^{17}O DOR spectra of (A) KH chloromaleate at 14.1 T, (B) KH maleate at 14.1 T, (C) K_2 chloromaleate at 14.1 T, and (D) K_2 chloromaleate at 8.45 T. The asterisk (*) represents δ_{dor}.

observed at 197.2 ± 0.5 ppm can be assigned to O−H oxygens. The larger width of the signal is probably a result of the low outer rotor speeds available and the absence of ^{1}H-decoupling.

TABLE 2: Comparison between ^{17}O NMR Parameters Obtained from MAS and DOR Experiments

				DOR expt.		MAS expt.	
carboxylic compounds	site	B_o/T	δ_{dor}/±0.5 ppm	δ_{iso}/±0.5 ppm	P_Q/±0.1 MHz	δ_{iso}/±2 ppm	P_Q/±0.2 MHz
KH maleate	C═O	14.1	256.3	319.3[a]	8.3[a]	321	8.3
	O−H	14.1	197.2	232.5[a]	6.2[a]	235	6.2
KH chloromaleate	C═O1	14.1	252.0	315.7[a]	8.4[a]	315	8.4
	C═O4	14.1	254.0	317.7[a]	8.4[a]	317	8.4
	O−H	14.1	188.8	226.8[a]	6.5[a]	228	6.5
K_2 chloromaleate	O═C1═O	14.1	237.5	288.1[b1]	7.5[b1]	288	7.4
		8.45	147.5				
	O═C2═O	14.1	232.1	282.1[b1]	7.4[b1]	283	7.4
		8.45	143.3				
	O═C1═O	14.1	237.5	290.5[b2]	7.6[b2]		
		8.45	143.3				
	O═C2═O	14.1	232.1	279.7[b2]	7.2[b2]		
		8.45	147.5				

[a] Deduced from eq 4 and the quadrupolar parameters reported in Table 1. [b] Deduced from eqs 5 and 6: (1) parallel δ_{dor1} and δ_{dor2} set, (2) cross δ_{dor1} and δ_{dor2} set.

The ^{17}O DOR spectrum (Figure 7A) of KH chloromaleate is similar to that of KH maleate with, however, two sharp signals with line widths of about 80 Hz appearing in the C═O spectral region at 252 and 254 ppm. The resolution available in this ^{17}O DOR experiment is very high, with the two resonances only 2 ppm apart being well resolved. On the basis of spectral comparison between the KH maleate and KH chloromaleate, one can assign the resonance at 252 ppm to C═O1 which is closer to the chlorine atom and 254 ppm to C═O4 of the chloromaleate.

Another advantage of the DOR experiment is that the observed DOR resonance position (δ_{dor}) can be used to confirm the ^{17}O NMR parameters obtained from MAS experiments or vice versa. This is because δ_{dor} depends on the applied magnetic field through second-order quadrupole effects for a spin $I = {}^5/_2$ nucleus as

$$\delta_{dor}(\text{ppm}) = \delta_{iso}(\text{ppm}) - \frac{3}{500}\frac{{P_Q}^2}{{\upsilon_o}^2} \times 10^6 \qquad (4)$$

where υ_o is the Larmor frequency, and $P_Q = \chi_q(1 + \eta_q^2/3)^{1/2}$. Through the use of the above equation and the quadrupolar parameters reported in Table 1, the isotropic chemical shifts of the different oxygen sites in KH maleate and KH chloromaleate are calculated and summarized in Table 2. The calculated δ_{iso} values are consistent with the values obtained on the basis of the NMR parameters determined from the ^{17}O MAS spectra.

As shown in Figure 3C, the ^{17}O MAS spectrum of K_2 chloromaleate exhibits a strong resonance with a center of gravity at about 240 ppm. Unfortunately, no crystal structure has been reported for K_2 chloromaleate to assist the spectral analysis. However, one can assume that there would be no H-bonds present because of the lack of a hydroxyl hydrogen, which is replaced by potassium ions. As a result, the oxygen should interact with the neighboring potassium ions. Furthermore, due to the lack of hydrogen, K_2 chloromaleate should also show resonant bonding structures, where the π-electrons delocalize between the C═O and C−O bonds, resulting in two sets of similar carboxylate oxygen sites (O═C1═O and O═C2═O). For this reason, the observed resonance in the ^{17}O MAS spectrum (Figure 3C) should consist of just two overlapping ^{17}O signals, one from each of the pairs of oxygens in the resonant structure attached to C1 and C2. To resolve these oxygen sites, a ^{17}O DOR spectrum was recorded at 14.1 T (Figure 7C). In the DOR spectrum, there are three distinct resonances, two sharp and one broad. The sharp signals are separated by ∼5 ppm at 237.5 and 232.1 ppm, which correspond to the two different pairs of O═C═O oxygens. The broad signal at 214.1 ppm is assigned to some other, as yet unidentified, species in the sample. With the two distinct sharp resonances in DOR, it is now possible to obtain site-specific information. To determine the NMR parameters, a DOR spectrum was recorded at a lower magnetic field (at 8.45 T) and is shown in Figure 7D, exhibiting two sharp signals at 147.5 and 143.3 ppm. The δ_{dor} changes observed between the 14.1 and 8.45 T spectra can be analyzed according to[46]

$$\delta_{iso} = \frac{{\nu_{o1}}^2\delta_{dor1} - {\nu_{o2}}^2\delta_{dor2}}{{\nu_{o1}}^2 - {\nu_{o2}}^2} \qquad (5)$$

and

$${P_Q}^2 = \frac{500}{3}{\upsilon_{o1}}^2{\upsilon_{o2}}^2\left(\frac{\delta_{dor1} - \delta_{dor1}}{{\upsilon_{o1}}^2 - {\upsilon_{o2}}^2}\right) \times 10^{-6} \qquad (6)$$

where δ_{dor1} and δ_{dor2} are the positions of the observed DOR resonances at the different fields. By the use of eqs 5 and 6, δ_{iso} and P_Q can be determined, and the results are reported in Table 2. With DOR data obtained at only two fields, it is possible to derive two sets of NMR interaction parameters: those where the two corresponding positions are joined (so that the lines are as parallel as possible) or the case when the extremes are connected (so that the lines cross over). Both possibilities are given in Table 2. Starting from the ^{17}O NMR parameters calculated from DOR by joining the "parallel" configuration, a set of ^{17}O NMR parameters can be deduced in excellent agreement with the MAS spectrum shown in Figure 3C. The results are summarized in Table 1. On the basis of the previous assignments on the KH chloromaleate, O═C2═O oxygens are probably those in closest proximity to the chlorine atom. It should be noted that the additional broader signal seen in the DOR data contributes only a small amount to the MAS spectrum and can be readily removed by spectral subtraction in the MAS data since it has a much shorter T_1. It is interesting to note that the isotropic chemical shift for the resonant carboxylate oxygens (O═C═O) is intermediate to that of carbonyl (C═O) and hydroxyl (O−H) oxygens. To the best of our knowledge, this is the first solid-state ^{17}O NMR data reported for such a resonant bonding structure in a carboxylate group. Gerothanassis et al.[58] have reported an upfield ^{17}O chemical shift of the deprontonated amino acids in solution.

TABLE 3: Spectral Resolution Comparison of ^{17}O MAS, 3QMAS, and DOR on KH Chloromaleate Solid at 14.1 T

oxygen sites	$\delta_{iso}/\pm 2$ ppm	$\delta_{3Q}/\pm 2$ ppm	$\delta_{DOR}/\pm 0.5$ ppm	$\Delta\upsilon_{MAS}$/Hz	$\Delta\upsilon_{3Q}$/Hz	$\Delta\upsilon_{DOR}$/Hz
C═O	315, 317	204	252.0, 254.0	12200 ± 200	700 ± 50	80 ± 5
O−H	228	223	188.8	6500 ± 100	1200 ± 50	600 ± 50

As mentioned previously, the weaker quadrupolar interactions and downfield shifts observed for O−H oxygens in KH maleate, KH chloromaleate, and K_2 chloromaleate are probably attributed to the fact that the oxygens are interacting with potassium ions. A similar metal effect is also observed for LiH phthalate·MeOH. As shown in the crystal structure, Figure 4C, LiH phthalate·MeOH[54] consists of one intramolecular hydrogen bond between two O−H oxygens, O2 and O3, with an O2···O3 distance of 2.390 Å. In addition, the C═O and O−H oxygens also have weak interactions with the neighboring lithium ions, at ca. 2.31 and 2.10 Å, respectively. As a result, both C═O and O−H sites show smaller χ_q values and downfield shifts of δ_{iso}: [C═O] $\delta_{iso} = 273 \pm 5$ ppm, $\chi_q = 7.35 \pm 0.10$ MHz, and $\eta_q = 0.30 \pm 0.10$; [O−H] $\delta_{iso} = 225 \pm 5$ ppm, $\chi_q = 6.47 \pm 0.10$ MHz, and $\eta_q = 0.25 \pm 0.10$. Wu and co-workers[27] reported the same trend for the O−H site in KH dibenzoate, where the K···O distances are ca. 2.8 Å.[55] It would be interesting to carry out a systematic study to further explore the metal effects on oxygen via ^{17}O NMR, because metal−oxygen interactions play important physiological roles in many biological systems, such as Fe···O in heme proteins[56] and Mg···O in chlorophyll.[57]

It is also worth comparing these results with the our preliminary results on phthalic acid and some phthalate salts.[35] The data on phthalic acid was unequivocal and agrees with what is seen here. For LiH phthalate·$2H_2O$, a strong signal was seen at ∼45 ppm and assigned to oxygen with a strong hydrogen-bond. Given the results observed here, it may be that the weak signals in that sample observed at ∼250 ppm are the carboxyl and hydroxyl oxygens and that the 45 ppm peak corresponds to hydrate species that have previously been observed in this vicinity.[18]

Spectral Resolution of 3QMAS and DOR. As clearly demonstrated from the previous section, both ^{17}O 3QMAS and DOR NMR experiments can effectively remove the second-order quadrupolar broadening and significantly increase the spectral resolution compared to the conventional ^{17}O MAS experiment. To make a comparison for $I = {}^5/_2$ nuclei between 3QMAS and DOR, we define the observed 3Q isotropic position (δ_{3Q}) as follows[46]

$$\delta_{3Q}(\text{ppm}) = \delta_{iso}(\text{ppm}) + \frac{3}{850}\frac{{P_Q}^2}{{\upsilon_L}^2} \times 10^6 \qquad (7)$$

and δ_{dor} was previously given in eq 4. The observed isotropic positions from MAS, 3QMAS, and DOR spectra for KH chloromaleate and their corresponding line widths are reported in Table 3. The observed line widths for δ_{3Q} are found to be an order of magnitude smaller than that observed in MAS. Here, even narrower signals are observed in the DOR spectrum. It is easier to obtain higher spectral resolution from DOR compared to MQMAS because it is a one-dimensional experiment which does not require a lengthy acquisition in the second (t_1) dimension where the signal may be weak. Nonetheless, both ^{17}O 3QMAS and DOR NMR experiments are highly suitable for studying oxygen sites in organic/bio-organic materials and give site-specific information with significantly enhanced resolution compared to MAS.

Theoretical Estimation of ^{17}O NMR Parameters. The experimental data observed above shows large ranges associated with both the isotropic chemical shift and quadrupole coupling constant, suggesting that individual oxygen sites that experience different structural environments can be readily distinguished. To gain a better understanding of the correlation between the observed ^{17}O NMR parameters and the surrounding oxygen environments, extensive quantum mechanical ^{17}O NMR calculations have been carried out.

Wu and co-workers[22−27] have recently reported that DFT provides useful calculations of ^{17}O chemical shielding and electric field gradient, using B3LYP level theory with a 6-311++G(d,p) basis set. In the present study, calculations of the same level were carried out on carboxylic oxygens to give the tensor components of the ^{17}O chemical shielding (σ_{ii}) and electric field gradients (q_{ii}). These σ_{ii} and q_{ii} components are directly related to the parameters (δ_{iso}, χ_q, and η_q) obtained from NMR spectroscopy; see eqs 1−3. The calculated results are tabulated in Table 4. Furthermore, the theoretical calculations give the sign of the EFG, whereas NMR experiments can only deduce absolute values. Figure 8 shows good agreement between the experimental and calculated values of δ_{iso} ($R^2 = 0.94$, standard deviation (sd) = 15 ppm), and of χ_q ($R^2 = 0.80$, sd = 0.4 MHz). However, the slopes found for the δ_{iso} (0.82) and χ_q (0.70) data indicate that the calculated values are overestimates. Wu and co-workers[26] also reported that the B3LYP calculations overestimate both the ^{17}O paramagnetic shielding and the electric field gradient for the target oxygen sites in nucleic acid bases and amide compounds. While part of the discrepancy between the experimental and calculated values is related to the nature of B3LYP calculations,[22−27] the cluster size used in the calculations[26] and the uncertainty of the hydrogen positions in X-ray crystal structures[59] will also affect the results. For example, the calculated ^{17}O shielding and EFG values for the C═O oxygen in oxalic acid changed by 10 ppm and 0.2 MHz toward the experimental values when the cluster size used in the B3LYP calculations was increased from first-coordination species (6 waters) to second-coordination species (12 waters and 4 oxalic acids), and Gervais et al.[49] found that using the neutron rather than the X-ray structure for L-alanine changed the ^{17}O shift by ∼8 ppm. Nevertheless, the calculations by B3LYP/6-311++G(d,p) confirm the NMR spectral assignments listed in Table 1. One advantage of ^{17}O NMR calculations over the ^{17}O NMR experiments is that the theoretical calculations can generally distinguish between the C═O and O−H oxygen sites in a carboxylic group by the sign of the χ_q values, whereas experimentally there is a nearly continuous variation in shift and the χ_q values overlap. It is found that a negative value corresponds to the O−H sites with a positive value for C═O. The difference in sign can probably be attributed to the σ- and π-bonding characteristics in C−O and C═O, respectively.

Hydrogen-Bond Effects on ^{17}O Shielding and EFG. On the basis of the above calculations, it is clear that the B3LYP/6-311G++(d,p) level of theory can yield a reasonable estimate of the ^{17}O NMR parameters. As seen in Tables 1 and 4, the different values observed for ^{17}O shielding and EFG of the oxygen sites in carboxylic groups must arise from differences in the surrounding environment. Besides the covalent bonds (C═O or C−O) to carbon that contribute to the different ^{17}O chemical shift regions, the oxygens also experience H-bonds, either of inter- or intramolecular form. To explore the influence

TABLE 4: Calculated ^{17}O NMR Parameters for Carboxylic Compounds at B3LYP/6-311++G(d,p)

carboxylic compounds	site	r(C═O···H−O)/Å	χ_q/MHz	η_q	δ_{iso}/ppm	χ_q[b]/MHz	η_q[b]	ref[c]
maleic acid	C═O1	1.596	9.18	0.11	343.7	7.480	0.25	50
	O4−H	1.596	−7.91	0.17	171.9	−6.935	0.05	50
	C═O3	1.661	9.79	0.09	369.0	8.545	0.085	50
	O2−H	1.661	−7.91	0.13	171.5	−7.175	0.085	50
chloromaleic acid	C═O5	1.737	8.13	0.48	327.2			*d*
	O6−H	1.737	−9.05	0.18	158.3	5.447	0.717	*d*
	C═O2	1.768	11.16	0.39	333.1			*d*
	O1−H	1.768	−8.95	0.33	161.2			*d*
KH maleate	C═O		9.54	0.13	349.8			52
	O−H	1.218[e]	−6.68	0.44	239.8	6.074	0.589	52
KH chloromaleate	C═O1		9.61	0.14	296.5			53
	C═O4		9.36	0.16	300.1			53
	O−H	1.205[e]	−6.89	0.49	224.2	6.330	0.580	53
LiH phthalate·MeOH	C═O	1.600	8.66	0.39	272.2			54
	O−H	1.227[e]	−6.83	0.66	244.5			54
phthalic acid	C═O	1.735	8.95	0.23	347.3	7.078	0.405	51
	O−H	1.735	−8.27	0.27	175.8	−7.173	0.147	51
oxalic acid·2H_2O	C═O	1.795	9.86	0.02	334.9	8.471	0.00	61
	O−H	1.513	−7.72	0.12	191.5	−7.454	0.160	61
KH dibenzoate[f]	C═O		8.96	0.22	301.2			55
	O−H	1.255[e]	−5.97	0.58	229.3	6.165	0.591	55
chloroacetic acid	C═O	1.920	9.75	0.03	355.9	8.207	0.157	62
	O−H	1.920	−8.23	0.17	130.5	−7.494	0.216	62
fumaric acid	C═O	2.002	10.37	0.01	374.4	8.226	0.125	63
	O−H	2.002	−8.84	0.15	108.9	−7.400	0.185	63
formic acid	C═O	1.762	9.81	0.05	354.9	7.818	0.07	64
	O−H	1.762	−7.63	0.13	167.0	−6.900	0.077	64
p-chlorobenzoic acid	C═O	1.719	9.25	0.23	323.5	6.113	0.769	65
	O−H	1.719	−8.37	0.18	153.4	−6.409	0.387	65
m-chlorobenzoic acid	C═O	1.761	9.49	0.15	321.9	6.440	0.565	66
	O−H	1.761	−9.13	0.06	147.3	−6.610	0.25	66
acrylic acid	C═O	1.703	9.54	0.14	330.9	7.565	0.31	67
	O−H	1.703	−8.24	0.15	146.9	−7.195	0.166	67
aspirin	C═O	1.559	8.66	0.29	302.2	6.793	0.551	68
	O−H	1.559	−8.41	0.14	183.5	−6.933	0.000	68
isophthalic acid	C═O	1.701	8.90	0.26	311.3	7.198	0.416	69
	O−H	1.701	−8.07	0.16	165.8	−6.765	0.155	69

[a] The parameters are compared with the previous reported NQR data. [b] NQR data from ref 70. [c] Structural reference. [d] This work. [e] The H-bond interaction between C−O−and O−H oxygens. [f] From ref 27.

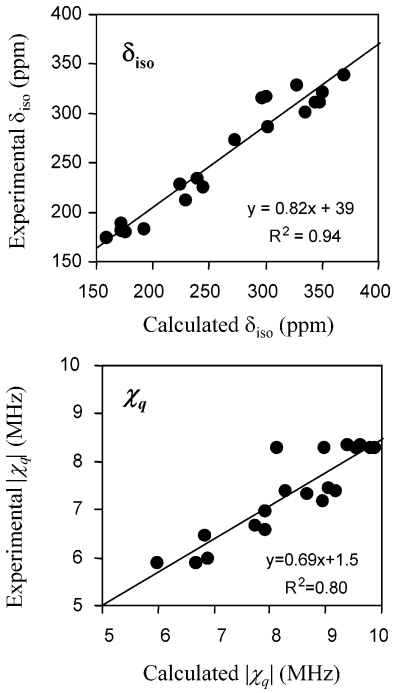

Figure 8. Comparison between experimental and calculated ^{17}O NMR parameters (δ_{iso} and χ_q). The calculated values are computed at the B3LYP/6-311++G(d,p) level.

of H-bonds on the oxygen sites, the set of ^{17}O NMR parameters for carboxylic compounds were extended by estimating the ^{17}O shielding and EFG, using B3LYP/6-311G++(d,p), for a series of carboxylic acid compounds with their C═O···H−O distance ranging from 1.2 to 2.0 Å. Some carboxylic compounds examined here have been studied by nuclear quadrupolar resonance (NQR), and their EFGs have been previously reported.[70] As found earlier, the calculated EFG values are uniformly ∼20% too large compared with experimental NQR values ($R^2 = 0.9$).

Figure 9 shows the calculated ^{17}O δ_{iso} values, reported in Table 4, for C═O and O−H sites vs the H-bond distance (C═O···H−O). For C═O oxygens, δ_{iso} increases (downfield shifts) as the H-bond distance increases and the bond strength decreases. In contrast, δ_{iso} of O−H oxygen decreases (upfield shifts) as the H-bond strength decreases. There is an excellent correlation between the O−H shift and the bond length ($R^2 = 0.94$, sd = 9 ppm). The C═O shift increases with decreasing bond length but with much more scatter ($R^2 = 0.37$, sd = 22 ppm) than for the O−H. Part of the observed scatter could be due to the uncertainty of the hydrogen positions in the crystal structures. In addition, for the C═O oxygens (the H-acceptor), generally more than one H-interaction is involved. Since only the well-defined H-bond is used in the correlation, the correlation with the H-bond strength is more scattered. In contrast, the O−H oxygen has one, less variable, H-bond involved in the correlation. This suggests that the O−H shift might be a useful and sensitive indicator of H-bond strength. Reuben[71] also reported similar H-effects on ^{17}O chemical shifts in solution. The O−H oxygen experiences a greater downfield shift when it acts as proton donor than that when it serves as proton acceptor. Correlations are also found between ^{17}O EFG and H-bond strength for both O−H and C═O, with that for O−H not being

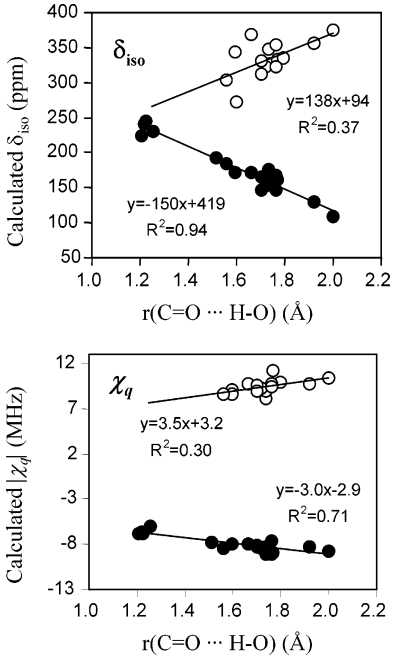

Figure 9. Correlations between the calculated ^{17}O NMR parameters (δ_{iso} and χ_q) and the H-bond strength (C═O···H−O). The calculated values are computed at the B3LYP/6-311++G(d,p) level. The solid and open circles represent O−H and C═O oxygen sites, respectively.

as good as that with the shift ($R^2 = 0.71$, sd = 0.5 MHz), while for C═O, the correlations are comparable. The correlation shown in Figure 9 demonstrates that the weakening of H-bonds (C═O···H−O) leads to an increase in χ_q values for C═O oxygen sites and a decrease for O−H oxygen. Similar trends of the ^{17}O shielding and EFG have been reported by Yates et al.[37] who observed increasing values of δ_{iso} and χ_q for C═O oxygen as the H-bonds weaken in glutamate solids and by Seliger[72] for the NQR data of the oxygen sites in carboxylic compounds.

To further explore the correlations between the ^{17}O NMR parameters and the H-bond environments, a series of ^{17}O shielding and EFG calculations were performed on a model that represents the intermolecular H-bonding motif. In this model, two acrylic acid molecules were used where their carboxylic oxygens interact by H-bonding and form a dimer molecule, as shown in Figure 10A. The two H-bonds (C═O···H−O) in the dimer molecule were varied from 1.433 to 2.874 Å, while keeping the H−O distance constant at a standard O−H value, 0.96 Å. ^{17}O NMR parameters of C═O and O−H oxygens were calculated, as one molecule moved away from the other. The model was constructed from the original crystal structure of acrylic acid[67] without structural optimization. This model allows for a qualitative study of the influence on the ^{17}O NMR parameters of a "single" H-bonding interaction, whereas experiment is restricted by the crystal structures and often involves multiple H-interactions. Both ^{17}O shielding and EFG were calculated at a B3LYP/6-311++G(d,p) level of theory. The results are reported in Table 5.

As shown in Figure 10B, the behavior of the ^{17}O shielding and EFG with the H-bond strength (C═O···H−O) is similar to those found in Figure 9. The ^{17}O shielding of the C═O oxygen shifts downfield, from 320 to 360 ppm, as the acrylic molecule moves further away from the target C═O oxygen site. In contrast, the shielding for O−H shifts upfield, from 160 to 130 ppm. The absolute value of EFG is found to increase slightly as the H-bond strength weakens for both C═O and O−H oxygen

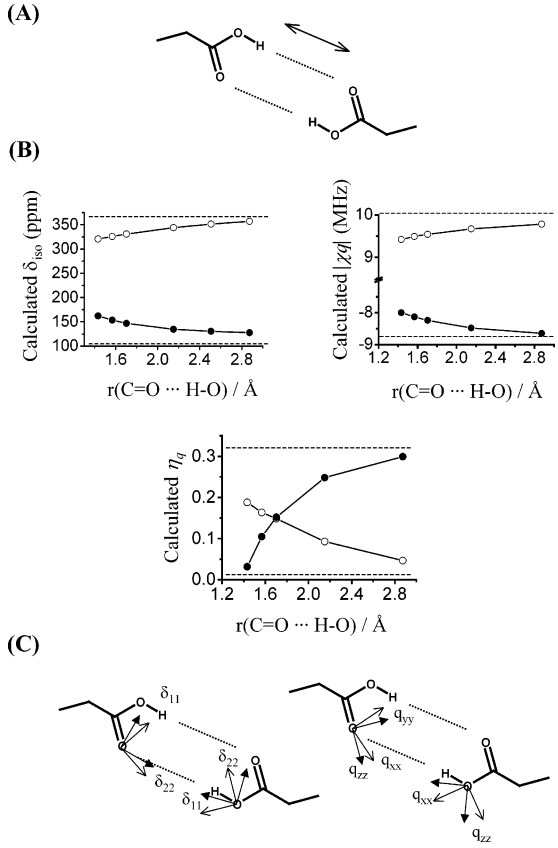

Figure 10. (A) Dimer model, acrylic acid, of intermolecular H-bonding used in the calculations. See text for detailed discussion. (B) The correlations between the calculated ^{17}O NMR parameters (δ_{iso}, χ_q, and η_q) and the H-bond strength (C═O···H−O). The NMR parameters are computed at the B3LYP/6-311++G(d,p) level. The dashed horizontal lines represent the values for an isolated acrylic acid. The solid and open circles represent O−H and C═O oxygen sites, respectively. (C) The tensor orientations of the calculated ^{17}O shielding and EFG on C═O and O−H oxygens: thick arrows correspond to a dimer with strong H-bonding, r(C═O···H−O) = 1.433 Å, whereas thin arrows correspond to a dimer with weak H-bonds, r(C═O···H−O) = 2.874 Å.

sites, from 9.4 to 9.8 and 8.0 to 8.5 MHz, respectively. The asymmetry parameter of the C═O oxygen is found to become more axial as the H-bond strength weakens, whereas for the O−H oxygen it becomes less axial. The larger change in ^{17}O shielding suggests that this is more sensitive to the H-bond environment than the EFG.

Another advantage of quantum calculations of NMR parameters is that they provide tensor orientations of both ^{17}O EFG and shielding at the oxygen sites with respect to the molecular frame. The calculated values of the principal tensor components for both shielding (δ_{11}, δ_{22}, and δ_{33}) and EFG (q_{xx}, q_{yy}, and q_{zz}) at the target sites for a series of H-bond strengths are reported (Table 5). Figure 10C shows the orientation of the tensor components with respect to the molecular frame. For shielding tensors, the largest shielding component, δ_{33}, for C═O and O−H oxygen sites are both perpendicular to the molecular plane, whereas the two smallest shielding components, δ_{11} and δ_{22}, lie on the same molecular plane. In particular, the δ_{11} component of O−H is nearly parallel with only ~5° deviation to the H-bond (O···H−O), for a strong H-bond interaction, with a C═O··· H−O distance of 1.433 Å. δ_{11} moves further away from the H-bond as the H-bond interaction weakens to 2.874 Å apart. For such weak interactions, the δ_{11} component is ca. 31° from the H-bond. Similar observations also relate to δ_{22} at the C═O

TABLE 5: Calculated ^{17}O Shielding and EFG Tensor Components of C═O and O−H Oxygens in an Intermolecular H-bonding Model of Acrylic Acid at B3LYP/6-311++G(d,p)[a]

r(C═O···H−O)/ Å	r(O···O)/ Å	site	δ_{11}/ ppm	δ_{22}/ ppm	δ_{33}/ ppm	δ_{iso}/ ppm	CSA[b]/ ppm
1.433	2.383	C═O	537.5	440.6	−15.7	320.8	553.2
		O−H	333.1	58.0	62.3	162.3	270.8
1.568	2.518	C═O	543.8	450.4	−16.5	325.9	560.3
		O−H	324.7	79.6	56.2	153.5	268.5
1.703	2.652	C═O	551.2	458.3	−16.7	330.9	567.9
		O−H	318.2	66.8	55.5	146.9	262.7
2.150	3.100	C═O	572.7	475.5	−15.7	344.2	588.4
		O−H	304.2	60.1	39.9	134.7	264.3
2.874	3.824	C═O	596.6	488.8	−13.9	357.1	610.5
		O−H	292.7	67.2	23.0	127.6	269.7
monomer		C═O	623.9	501.8	−15.3	370.1	639.2
		O−H	283.9	65.3	14.6	121.3	269.3

r(C═O···H−O)/ Å	r(O···O)/ Å	site	q_{xx}/ au[c]	q_{yy}/ au[c]	q_{zz}/ au[c]	χ_q/ MHz	η_q
1.433	2.383	C═O	−0.61	−0.89	1.51	9.42	0.19
		O−H	0.62	0.66	−1.28	−8.00	0.03
1.568	2.518	C═O	−0.63	−0.88	1.52	9.49	0.16
		O−H	0.58	0.72	−1.30	−8.13	0.14
1.703	2.652	C═O	−0.65	−0.88	1.53	9.54	0.15
		O−H	0.56	0.76	−1.32	−8.24	0.15
2.150	3.100	C═O	−0.70	−0.84	1.55	9.67	0.09
		O−H	0.51	0.88	−1.52	−8.48	0.25
2.874	3.824	C═O	−0.74	−0.82	1.57	9.78	0.04
		O−H	0.48	0.90	−1.39	−8.65	0.30
monomer		C═O	−0.79	−0.80	1.60	10.01	0.01
		O−H	0.46	0.93	−1.40	−8.75	0.32

[a] See text for detailed discussion. [b] CSA = $\delta_{11} - \delta_{33}$. [c] Atomic units, 1 au = 9.717365 × 10^{21} V m^{-2}.

oxygen site. δ_{22} is only 4° from the H-bond when the C═O···H−O bond is 1.433 Å apart, and the δ_{22} shifts 26° away from the H-bond as the interaction becomes weaker. This is the first time that the changes of shielding tensor orientations are reported for different H-bond strengths. It is interesting to note that the shielding components δ_{11} and δ_{22}, of the O−H and C═O oxygens, respectively, line up nearly parallel to the H-bond and shift away as the interaction gets weaker. Wu and co-workers reported shielding tensors for C═O oxygen in urea[24] and KH dibenzoate.[27] Similar to our results, they reported that the δ_{11} component is perpendicular to the C═O bond and suggested that the shielding changes arise from $\sigma \rightarrow \pi^*$ and $\pi \rightarrow \sigma$ mixing. The largest shielding component at the carboxylate oxygens in glutamate is found to be perpendicular to the molecular plane.[37] In addition to the orientations of the ^{17}O shielding tensor, the chemical shift anisotropy (CSA), CSA = $\delta_{11} - \delta_{33}$, for the C═O oxygen is found to be much larger than that for the O−H oxygen. The CSA for the C═O oxygen increases from 550 to 610 ppm as the H-bond weakens, while very little change is observed for the O−H oxygen. The latter observation may be due to the fact that the calculation was done at a fixed O−H distance (0.96 Å) for all intermolecular H-bond (C═O···H−O) distances.

In contrast to the case for the ^{17}O shielding tensors, the EFG tensors for C═O and O−H have quite different orientations from one another. In particular, the EFG component that is perpendicular to the molecular plane is different for C═O and O−H oxygens. q_{yy} is found to be perpendicular to the molecular plane at the O−H oxygen for all C═O···H−O bond distances, whereas, q_{xx} is found to be perpendicular to the plane at the C═O oxygen for a dimer with a strong H-bond but switches to q_{zz} for a weak H-bond. At the O−H site, q_{xx} values are 10° and 50° off from the strong and weak C═O···H−O bonds, respectively. At the C═O site, q_{xx} is 30° off from the H-bond for the strong H-bond and q_{zz} is 62° for the weak H-bond. There is now a small, but nevertheless increasing, data set reporting the orientation of ^{17}O EFG tensors at oxygen sites in organic/bio-organic materials,[20−27,36,37,70,72] but there are still no completely unambiguous trends observed. More studies are needed to understand in detail the structural factors that influence the orientations of EFG tensors at the oxygen sites.

Conclusion

The present study has demonstrated the great potential of solid-state ^{17}O NMR spectroscopy for studying the oxygen sites in organic/biological molecules by examining several ^{17}O-enriched carboxylic compounds. Although high-quality ^{17}O MAS, 3QMAS, and DOR spectra for carboxylic compounds can often be obtained with 10% ^{17}O enrichment, higher ^{17}O enrichment levels are often desirable to enhance the NMR sensitivity particularly if 3QMAS is contemplated. Application of ^{17}O 3QMAS and DOR techniques can remove the intrinsic second-order quadrupolar broadening of the oxygen and reveal distinct resonances for different oxygen sites at high resolution. The line width of the isotropic resonances from both 3QMAS and DOR experiments is much reduced here compared to MAS, making it possible to obtain site-specific NMR information. The good correlation between isotropic shift and H-bond strength for O−H may find an application in determining bond strengths.

By the use of a quantum mechanical approach, the calculated ^{17}O NMR parameters (δ_{iso} and χ_q) were in reasonable agreement with the experimental values and showed monotonic correlations between the ^{17}O NMR parameters and the H-bond strength. A systematic study of the effects of H-bonding on ^{17}O shielding tensors was carried out. The δ_{11} and δ_{22} components at the O−H and C═O oxygen are found to be parallel with the strong H-bond but shift away as the H-bond weakens.

Acknowledgment. We thank EPSRC and the University of Warwick for partially supporting the NMR equipment at Warwick and the BBSRC for funding ^{17}O NMR through Grant BB/C000471/1 (2005-2008). A.W. thanks the NSERC of Canada for the Postdoctoral Fellowship Award (2005−2006) and Canada-UK Millennium Fellowship (2005−2006). We also thank Dr. G. Wu (Queen's University in Canada) for allowing us to access the HPVLC computers for the calculations. We would like to thank the referees who made some very helpful comments on the manuscript. The Royal Society is thanked for funding aspects of the initial stages of this work. A.S. would like to acknowledge the support of FP6 Project LSHG-CT-20040512052.

Supporting Information Available: CIF data for chloromaleic acid. This material is available free of charge via the Internet at http://pubs.acs.org.

References and Notes

(1) (a) Wüthrich, K. *Nat. Struct. Biol.* **1998**, *5*, 492. (b) Wüthrich, K. In *NMR-An alternative to X-ray crystallography for protein and nuclei acid structure determination*; Haase, A., Landwehr, G., Umbach, E., Eds.; World Scientific: Singapore, 1997; pp 242−257. (c) Wüthrich, K. In *NMR of Proteins and Nucleic Acids*; Wiley: New York, 1986. (d) Wider, G. *Biotechnology* **2000**, *29*, 1278.

(2) Lemaître, V.; Smith, M. E.; Watts, A. *Solid State Nucl. Magn. Reson.* **2004**, *26*, 215 and references therein.

(3) (a) Klemperer, W. G. *Angew. Chem., Int. Ed. Engl.* **1978**, *17*, 246. (b) Kintzinger, J. P. In *NMR Basic Principles and Progress*; Diehl, P., Fluck, E., Kosfeld, R., Eds.; Springer-Verlag: Berlin, 1981; Vol. 17, pp 1−65. (c) McFarlane, W.; McFarlane, H. C. E. In *Multinuclear NMR*; Mason, J., Ed.; Plenum Press: New York, 1987; Chapter 14, pp 403−416. (d) Boykin, D. W., Ed. *Oxygen-17 NMR Spectroscopy in Organic Chemistry*; CRC

Press: Boca Raton, FL, 1991. (e) Gerothanassis, I. P. In *Encyclopedia of Nuclear Magnetic Resonance*; Grant, D. M., Harris, R. K., Eds.; John Wiley and Sons: New York, 1996; pp 3430−3440. (f) Pearson, J. G.; Oldfield, E. In *Encyclopedia of Nuclear Magnetic Resonance*; Grant, D. M., Harris, R. K., Eds.; John Wiley and Sons: New York, 1996; pp 3440−3443. (g) Gerothanassis, I. P.; Vakka, C. *J. Org. Chem.* **1994**, *59*, 2341.

(4) Wu, G. *Biochem. Cell Biol.* **1998**, 429.

(5) Schramm, S.; Kirkpatrick, R. J.; Oldfield, E. *J. Am. Chem. Soc.* **1983**, *105*, 2483. (b) Schramm, S.; Oldfield, E. *J. Am. Chem. Soc.* **1984**, *106*, 2502. (c) Walter, T. H.; Turner, G. L.; Oldfield, E. *J. Magn. Reson.* **1988**, *76*, 106.

(6) Bastow, T. J.; Stuart S. N. *Chem. Phys.* **1990**, *143*, 359.

(7) Bastow, T. J.; Dirken, P. J.; Smith, M. E.; Whitfield, H. J. *J. Phys. Chem.* **1996**, *100*, 18539.

(8) MacKenzie, K. J. D.; Smith M. E. In *Multinuclear Solid State NMR of Inorganic Materials*; Pergamon Press: Oxford, U.K., 2002.

(9) (a) Timken, H. K. C.; Schramm, S. E.; Kirkpatrick, R. J.; Oldfield, E. *J. Phys. Chem.* **1987**, *91*, 1054. (b) Grandinetti, P. J.; Baltisberger, J. H.; Farnan, I.; Stebbins, J. F.; Werner, U.; Pines, A. *J. Phys. Chem.* **1995**, *99*, 12341. (c) Ashbrook, S. E.; Berry, A. J.; Wimperis, S. *J. Am. Chem. Soc.* **2001**, *123*, 6360. (d) Ashbrook, S. E.; Berry, A. J.; Wimperis, S. *J. Phys. Chem. B* **2002**, *106*, 773. (e) Ashbrook, S. E.; Berry, A. J.; Hibberson, W. O.; Steuernagel, S.; Wimperis, S. *J. Am. Chem. Soc.* **2003**, *125*, 11824.

(10) (a) Maekawa, H.; Florian, P.; Massiot, D.; Kiyono, H.; Nakamura, M. *J. Phys. Chem.* **1996**, *100*, 5525. (b) Dirken, P. J.; Kohn, S. C.; Smith, M. E.; van Eck, E. R. H. *Chem. Phys. Lett.* **1997**, *266*, 568. (c) Lee, S. K.; Stebbins, J. F. *J. Non-Cryst. Solids* **2000**, *270*, 260.

(11) (a) Dirken, P. J.; Smith, M. E.; Whitfield, H. J. *J. Phys. Chem.* **1995**, *99*, 295. (b) Pickup, D. M.; Mountjoy, G.; Holland, M. A.; Wallidge, G. W.; Newport, R. J.; Smith, M. E. *J. Mater. Chem.* **2000**, *10*, 1887. (c) Pickup, D. M.; Mountjoy, G.; Wallidge, G. W.; Newport, R. J.; Smith, M. E. *Phys. Chem. Chem. Phys.* **1999**, *1*, 2527. (d) Gervais, C.; Babonneau, F.; Smith, M. E. *J. Phys. Chem. B* **2001**, *105*, 1971.

(12) (a) Bull, L. M.; Cheetham, A. K.; Anupõld, T.; Reinhold, A.; Samoson, A.; Sauer, J.; Bussemer, B.; Lee, Y.; Gann, S.; Shore, J.; Pines, A.; Dupree, R., *J. Am. Chem Soc.* **1998**, *120*, 3510. (b) Bull, L. M.; Bussemer, B.; Anupõld, T.; Reinhold, A.; Samoson, A.; Sauer, J.; Cheetham, A. K.; Dupree, R. *J. Am. Chem. Soc.* **2000**, *122*, 4948.

(13) Du, L.-S.; Stebbins, J. F. *Solid State Nucl. Magn. Reson.* **2005**, *27*, 37 and references therein.

(14) (a) Zeyer, M.; Montagne, L.; Kostoj, G.; Palavit, G.; Prochnow, D.; Jaeger, C. *J. Non-Cryst. Solids* **2002**, *311*, 223. (b) Cherry, B. R.; Alam, T. M.; Click, C.; Brow, R. K.; Gan, Z. *J. Phys. Chem. B* **2003**, *107*, 4894. (c) Zeyer-Düsterer, M.; Montagne, L.; Palavit, G.; Jäger, C. *Solid State Nucl. Magn. Reson.* **2005**, *27*, 50.

(15) (a) Goc, R.; Ponnusamy, E.; Tritt-Goc, J.; Fiat, D. *Int. J. Pept. Protein Res.* **1988**, *31*, 130. (b) Goc., R.; Tritt-Goc., J.; Fiat, D. *Bull. Magn. Reson.* **1989**, *11*, 238.

(16) (a) Augspurger, J. D.; Dykstra, C. E.; Oldfield, E. *J. Am. Chem. Soc.* **1991**, *113*, 2447. (b) Oldfield, E.; Lee, H. C.; Coretsopoulos, C.; Adebodum, F.; Park, K. D.; Yang, S.; Chung, J.; Phillips, B. *J. Am. Chem. Soc.* **1991**, *113*, 8680. (c) Park, K. D.; Guo, K.; Adebodun, F.; Chiu, M. L.; Sligar, S. G.; Oldfield, E. *Biochemistry* **1991**, *30*, 2333. (d) Salzmann, R.; Kaupp, M.; McMahon, M. T.; Oldfield, E. *J. Am. Chem. Soc.* **1998**, *120*, 4771. (e) McMahon, M. T.; deDios, A. C.; Godbout, N.; Salzmann, R.; Laws, D. D.; Le, H.; Havlin, R. H.; Oldfield, E. *J. Am. Chem. Soc.* **1998**, *120*, 4784. (f) Godbout, N.; Sanders, L. K.; Salmann, R.; Havlin, R. H.; Wojdelski, M.; Oldfield, E. *J. Am. Chem. Soc.* **1999**, *121*, 3829.

(17) Lemaître, V.; de Planque, M. R. R.; Howes, A. P.; Smith, M. E.; Dupree, R.; Watts, A. *J. Am. Chem. Soc.* **2004**, *126*, 15320.

(18) Hu, J.; Chekmenev, E. Y.; Gan, Z.; Gor'kov, P. L.; Saha, S. Brey, W. W.; Cross, T. A. *J. Am. Chem. Soc.* **2005**, *127*, 11922.

(19) (a) Kuroki, S.; Takahashi, A.; Ando, I.; Shoji, A.; Ozaki, T. *J. Mol. Struct.* **1994**, *323*, 197. (b) Kuroki, S.; Ando, S.; Ando, I. *Chem. Phys.* **1995**, *195*, 107. (c) Yamauchi, K.; Kuroki, S.; Ando, I.; Ozaki, T.; Shoji, A. *Chem. Phys. Lett.* **1999**, *302*, 331.

(20) (a) Scheubel, W.; Zimmermann, H.; Haeberlen, U. *J. Magn. Reson.* **1985**, *63*, 544. (b) Zhang, Q. W.; Zhang, H. M.; Usha, M. G.; Wittebort, R. J. *Solid State Nucl. Magn. Reson.* **1996**, *7*, 147.

(21) Zhang, Q.; Chekmenev, E. Y.; Wittebort, R. J. *J. Am. Chem. Soc.* **2003**, *125*, 9140.

(22) Dong, S.; Yamada, K.; Wu, G. *Z. Naturforsch., A: Phys. Sci.* **2000**, *55*, 21.

(23) Wu, G.; Hook, A.; Dong, S.; Yamada, K. *J. Phys. Chem. A* **2000**, *104*, 4102.

(24) Dong, S.; Ida, R.; Wu, G. *J. Phys. Chem. A* **2000**, *104*, 11194.

(25) Wu, G.; Yamada, K.; Dong, S.; Grondey, H. *J. Am. Chem. Soc.* **2000**, *122*, 4215.

(26) (a) Wu, G.; Dong, S.; Ida, R.; Reen, N. *J. Am. Chem. Soc.* **2002**, *124*, 1768. (b) Yamada, K.; Dong, S.; Wu, G. *J. Am. Chem. Soc.* **2000**, *122*, 11602.

(27) Wu, G.; Yamada, K. *Solid State Nucl. Magn. Reson.* **2003**, *24*, 196.

(28) (a) Llor, A.; Virlet, J. *Chem. Phys. Lett.* **1988**, *152*, 248. (b) Mueller, K. T.; Sun, B. Q.; Chingas, G. C.; Zwanziger, J. W.; Terao, T.; Pines, A. *J. Magn. Reson.* **1990**, *86*, 470.

(29) (a) Samoson, A.; Lippmaa, E.; Pines, A. *Mol. Phys.* **1988**, *65*, 1013. (b) Chmelka, B. F.; Mueller, K. T.; Pines, A.; Stebbins, J.; Wu, Y.; Zwanziger, J. W. *Nature* **1989**, *339*, 42. (c) Wu, Y.; Sun, B. Q.; Pines, A.; Samoson, A.; Lippmaa, E. *J. Magn. Reson.* **1990**, *89*, 296.

(30) (a) Frydman, L.; Harwood, J. S. *J. Am. Chem. Soc.* **1995**, *117*, 5367. (b) Medek, A.; Harwood, J. S.; Frydman, L. *J. Am. Chem. Soc.* **1995**, *117*, 12779.

(31) Wu, G.; Dong, S. *J. Am. Chem. Soc.* **2001**, *123*, 9119.

(32) Gann, S. L.; Baltisberger, J. H.; Wooten, E. W.; Zimmermann, H.; Pines, A. *Bull. Magn. Reson.* **1994**, *16*, 68.

(33) Pike, K. J.; Lemaître, V.; Kukol, A.; Anupõld, T.; Samoson, A.; Howes, A. P.; Watts, A.; Smith, M. E.; Dupree, R. *J. Phys. Chem. B* **2004**, *108*, 9256.

(34) Lemaître, V.; Pike, K. J.; Watts, A.; Anupõld, T.; Samoson, A.; Smith, M. E.; Dupree, R. *Chem. Phys. Lett.* **2003**, *371*, 91.

(35) Howes, A. P.; Jenkins, R.; Smith, M. E.; Crout, D. H. G.; Dupree, R. *Chem. Commun.* **2001**, 1448.

(36) Bryce, D. L.; Eichele, K.; Wasylishen, R. E. *Inorg. Chem.* **2003**, *42*, 5085.

(37) Yates, J. R.; Pickard, C. J.; Payne, M. C.; Dupree, R.; Profeta, M.; Mauri, F. *J. Phys. Chem. A* **2004**, *108*, 6032.

(38) Jeffrey, G. A. *An Introduction to Hydrogen Bonding*; Oxford University Press: Oxford, U.K., 1997.

(39) *SHELXTL Crystal Structure Analysis Package, Bruker AXS, Analytical X-ray System*; Siemens: Madison, WI, 1997.

(40) Kunwar, A. C.; Turner, G. L.; Oldfield, E. *J. Magn. Reson.* **1986**, *69*, 124.

(41) *WinNuts for Windows 95/NT*, 1D Version − 19990111; Acorn NMR, Inc.

(42) For information about WSOLIDS, please contact Dr. Klaus Eichele, http://casgm3.anorg.chemie.uni-tuebingen.de/klaus/soft/index.html.

(43) Brown, S. P.; Wimperis, S. *J. Magn. Reson.* **1997**, *128*, 42.

(44) Samoson, A.; Lippmaa, E. *J. Magn. Reson.* **1989**, *84*, 410.

(45) Frisch, M. J.; Trucks, G. W.; Schlegel, H. B.; Scuseria, G. E.; Robb, M. A.; Cheeseman, J. R.; Zakrzewski, V. G.; Montgomery, J. A.; Stratmann, R. E.; Burant, J. C.; Dapprich, S.; Millam, J. M.; Daniels, A. D.; Kudin, K. N.; Strain, M. C.; Farkas, O.; Tomasi, J.; Barone, V.; Cossi, M.; Cammi, R.; Mennucci, B.; Pomelli, C.; Adamo, C.; Clifford, S.; Ochterski, J.; Petersson, G. A.; Ayala, P. Y.; Cui, Q.; Morokuma, K.; Malick, D. K.; Rabuck, A. D.; Raghavachari, K.; Foresman, J. B.; Cioslowski, J.; Ortiz, J. V.; Stefanov, B. B.; Liu, G.; Liashenko, A.; Piskorz, P.; Komaromi, I.; Gomperts, R.; Martin, R. L.; Fox, D. J.; Keith, T.; Al-Laham, M. A.; Peng, C. Y.; Nanayakkara, A.; Gonzalez, C.; Challacombe, M.; Gill, P. M. W.; Johnson, B.; Chen, W.; Wong, M. W.; Andres, J. L.; Head-Gordon, M.; Replogle, E. S.; Pople, J. A. *Gaussian 98*, revision A.6; Gaussian, Inc.: Pittsburgh, PA, 1998.

(46) Smith, M. E.; van Eck, E. R. H. *Prog. Nucl. Magn. Reson. Spectrosc.* **1999**, *34*, 159.

(47) Pyykkö, P. *Mol. Phys.* **2001**, *99*, 1617.

(48) Wasylishen, R. E.; Bryce, D. L. *J. Chem. Phys.* **2002**, *117*, 10061.

(49) Gervais, C.; Dupree, R.; Pike, K. J.; Bonhomme, C.; Profeta, M.; Pickard, C. J.; Mauri, F. *J. Phys. Chem.* **2005**, *109*, 6960.

(50) James, M. N. G.; Williams, G. J. B. *Acta Crystallogr, Sect. B* **1974**, *30*, 1249.

(51) Ermer, O. *Helv. Chim. Acta* **1981**, *64*, 1902.

(52) Darlow, S. F. *Acta Crystallogr.* **1961**, *14*, 1250.

(53) Ellison, R. D.; Levy, H. A. *Acta Crystallogr.* **1965**, *19*, 260.

(54) Küppers, H.; Kvick, A.; Olovsson, I. *Acta Crystallogr., Sect. B* **1981**, *37*, 1203.

(55) Skinner, J. M.; Stewart, G. M. D.; Speakman, R. E. *J. Chem. Soc.* **1954**, 180.

(56) Falk, J. E. In *Porphyrins and Metalloporphyrins*; Elsevier: Amsterdam, The Netherlands, 1975.

(57) Scheer, H. In *Chlorophylls*; CRC Press: Boca Raton, FL, 1991.

(58) Gerothanassis, I. P.; Hunston, R. N.; Lauterwein, *J. Magn. Reson. Chem.* **1985**, *23*, 659.

(59) Brin, J.; Poon, A.; Mao, Y.; Ramamoorthy, A. *J. Am. Chem. Soc.* **2004**, *126*, 8529.

(60) Bennett, A. E.; Rienstra, C. M.; Auger, M.; Lakshmi, K. V.; Griffin, R. G. *J. Chem. Phys.* **1995**, *103*, 6951.

(61) Sabine, T. M.; Cox, G. W.; Craven, B. M. *Acta Crystallogr., Sect. B* **1969**, *25*, 2437.

(62) Kanters, J. A.; Roelofsen, G.; Feenstra, T. *Acta Crystallogr., Sect. B* **1976**, *32*, 3331.

(63) Bednowitz, A. L.; Post, B. *Acta Crystallogr.* **1966**, *21*, 566.

(64) Nahringbauer, I. *Acta Crystallogr., Sect. B* **1978**, *34*, 315.
(65) Takazawa, H.; Ohba, S.; Saito, Y. *Acta Crystallogr., Sect. B* **1989**, *45*, 432.
(66) Gougoutas, J. Z.; Lessinger, L. *J. Solid State Chem.* **1975**, *12*, 51.
(67) Boese, R.; Blaser, D.; Steller, I.; Latz, R.; Baumen, A. *Acta Crystallogr., Sect. C* **1999**, *55*, 9900006.
(68) Wilson, C. C. *New J. Chem.* **2002**, *26*, 1733.
(69) Derissen, J. L. *Acta Crystallogr., Sect. B* **1974**, *30*, 2764.
(70) (a) Poplett, I. J. F.; Smith, J. A. S. *J. Chem. Soc., Faraday Trans.* **1981**, *77*, 1473. (b) Poplett, I. J. F.; Sabir, M.; Smith, J. A. S. *J. Chem. Soc., Faraday Trans.* **1981**, *77*, 1651. (c) Brosnan, S. G. P.; Edmonds, D. T.; Poplett, I. J. F. *J. Magn. Reson.* **1981**, *45*, 451.
(71) Reuben, J. *J. Am. Chem. Soc.* **1969**, *91*, 5725.
(72) Seliger, J. *Chem. Phys.* **1998**, *231*, 81.